Iterative Frequency-Domain Equalization for Single-Carrier Systems in Doubly-Dispersive Channels

Philip Schniter and Hong Liu
Dept. ECE, The Ohio State University, 2015 Neil Ave, Columbus, OH 43210
schniter.1@osu.edu, liu.523@osu.edu

***Abstract*— Frequency-domain equalization (FDE) offers an attractive alternative to time-domain equalization in systems that communicate over large-delay-spread channels. Traditionally, FDE leverages the fact that time-domain convolution is equivalent to frequency-domain multiplication and the fact that time/frequency conversion is efficiently handled by the fast Fourier transform (FFT). In doubly dispersive channels, i.e., quickly varying large-delay-spread channels, the traditional FDE methods fail due to the time-varying property of the channel. Here we present a new FDE that is based on Doppler channel shortening, soft iterative interference cancellation, and block decision feedback. Numerical simulations show that the proposed technique outperforms the well-known FIR-MMSE-DFE in both performance and complexity.** [1]

I. Introduction

In systems that communicate over large-delay-spread channels, the use of time-domain equalization (TDE) leads to expensive receivers. For example, North American terrestrial digital television is plagued by delay spreads on the order of hundreds of symbol intervals, requiring time-domain equalizers with hundreds of coefficients. Frequency-domain equalization (FDE) offers an attractive alternative. FDE leverages the fact that circular convolution in the time domain can be accomplished by pointwise multiplication in the frequency domain, and the fact that transformation to/from the frequency domain can be efficiently accomplished using the FFT algorithm. Roughly speaking, the processing complexity required for TDE is linear in the channel delay spread while for FDE it is logarithmic in the delay spread. Thus, FDE can lead to significant savings over TDE for long channels.

FDE is the principle idea behind orthogonal frequency division multiplexing (OFDM) [1] and single-carrier cyclic-prefix (SCCP) modulation [2]. Both OFDM and SCCP systems transmit data in blocks separated by guard intervals. The guard prevents inter-block interference, thereby simplifying receiver processing. The use of a cyclic-prefix (CP) guard makes the channel's dispersion act as a cyclic (rather than linear) convolution, implying that deconvolution can be accomplished through pointwise frequency-domain multiplication. When guards are *not* included, FDE can still be accomplished using overlap-add/save FFT algorithms (see, e.g., [3]).

The previously mentioned FDE techniques assume a delay-spread channel whose impulse response varies negligibly over the FFT block duration. Some applications, however, have channels with more significant time variation, i.e., significant Doppler *and* delay spreads. For such doubly-dispersive channels, the standard approach to FDE (i.e., pointwise frequency-domain multiplication) is inadequate due the presence of Doppler-induced inter-carrier interference (ICI). In response, several equalization schemes for doubly-dispersed CP-OFDM (e.g., [4]–[7]) and SCCP (e.g., [8]) have been proposed. These algorithms, however, assume block-based transmissions with an adequate inter-block guard interval. For single-carrier *continuous-stream* modulation over doubly-dispersive channels, less work has been done (see, e.g., [9]).

In this paper we present an iterative frequency-domain equalizer (IFDE) for a continuous finite-alphabet stream corrupted by a noisy and doubly-dispersive channel. In brief, the algorithm parses the received time-domain signals into blocks, which are then transformed into the frequency domain using the FFT. By non-rectangularly windowing prior to the FFT, the quickly-varying channel response is transformed into a sparse Doppler response, making low-complexity frequency-domain equalization possible. Time-domain symbol estimates then result from a subsequent application of the FFT. While one could stop here, our algorithm exploits the symbols' finite-alphabet property through further processing stages of iterative soft-interference cancellation. Since the finite-alphabet property resides in the time-domain and the sparse channel property resides in the frequency domain, our algorithm alternates between these two domains to achieve its final result. Throughout, we assume the channel is perfectly known.

We use the following notation. Transpose is denoted by $(\cdot)^t$, conjugate by $(\cdot)^*$, and conjugate transpose by $(\cdot)^H$. The identity matrix is denoted by $\boldsymbol{I}$, and the k^{th} column of the the identity matrix by $\boldsymbol{i}_k$. The element in the m^{th} row and n^{th} column of matrix $\boldsymbol{B}$ is denoted by $[\boldsymbol{B}]_{m,n}$, where row/column indices begin with zero. The diagonal matrix created from vector $\boldsymbol{b}$ is denoted by $\mathcal{D}(\boldsymbol{b})$, and the circulant matrix with first column $\boldsymbol{b}$ by $\mathcal{C}(\boldsymbol{b})$. The $N \times 1$ vector created from the i^{th} sub-diagonal of $N \times N$ matrix $\boldsymbol{B}$ is denoted by $\mathrm{diag}_i(\boldsymbol{B})$, i.e., $[\mathrm{diag}_i(\boldsymbol{B})]_k = [\boldsymbol{B}]_{\langle k+i \rangle_N,k}$ for $k \in \{0,1,\ldots,N-1\}$. Expectation is denoted by $\mathrm{E}\{\cdot\}$ and covariance by $\mathrm{Cov}\{\boldsymbol{b},\boldsymbol{c}\} := \mathrm{E}\{\boldsymbol{b}\boldsymbol{c}^H\} - \mathrm{E}\{\boldsymbol{b}\}\,\mathrm{E}\{\boldsymbol{c}^H\}$. Finally, the Kronecker delta is denoted by δ_m, the modulo-N operation by $\langle\cdot\rangle_N$, and element-wise matrix multiplication by $\odot$.

[1]This work is supported in part by NSF CAREER Grant CCR-0237037.

II. System Model

Consider a single-carrier modulation system where a stream of finite-alphabet symbols $\{s_n\}$ is transmitted over a noisy linear time-varying (LTV) multipath channel. The channel is described by its time-variant discrete impulse response $h_{n,l}$, defined as the time-n response to an impulse applied at time $n-l$. We assume a causal impulse response of length N_h. The signal observed by the receiver is

$$r_n = \nu_n + \sum_{l=0}^{N_h-1} h_{n,l} s_{n-l} \tag{1}$$

where ν_n denotes samples of zero-mean circular white Gaussian noise (CWGN) with variance σ^2. We assume wide-sense stationary uncorrelated scattering (WSSUS) [10] so that $\mathrm{E}\{h_{n,l} h^*_{n-q,l-m}\} = \gamma_q \sigma_l^2 \delta_m$. Here, γ_q denotes the normalized autocorrelation (i.e., $\gamma_0 = 1$) and σ_l^2 the variance of the channel at delay l^{th}.

The remainder of this section establishes the block-based frequency-domain equivalent of (1). At each frame index $i \in \mathbb{Z}$, the receiver windows an iN-shifted version of the time-domain observation $\{r_n\}$ and applies a discrete Fourier transform (DFT) with frequency spacing $\frac{2\pi}{PN}$, yielding the i^{th}-frame frequency domain observation $\{x_d(i)\}_{d=0}^{PN-1}$:

$$x_d(i) = \frac{1}{\sqrt{PN}} \sum_n r_{iN+n} b_n e^{-j\frac{2\pi}{PN}dn}. \tag{2}$$

Note that the window length is arbitrary. Say, for convenience,

$$s_n(i) := s_{iN+n}, \quad n \in \{0,\dots,PN-1\} \tag{3}$$
$$a_n := \begin{cases} 1 & n \in \{0,\dots,PN-1\}, \\ 0 & \text{else}, \end{cases}$$

noting that $\{a_n\}$ is a PN-length rectangular window and that

$$s_{iN+n} = \sum_{\ell=-\infty}^{\infty} s_{\langle n \rangle_{PN}}(i-P\ell)\, a_{\ell PN+n}. \tag{4}$$

Equation (4) says that, for a particular i, the transmitted sequence $\{s_{iN+n}\}$ can be constructed using PN-sample shifts of the disjoint subsequences $\{s_n(i-P\ell)\}_{n=0}^{PN-1}$ for $\ell \in \mathbb{Z}$. Combining (1)-(4), we find

$$x_d(i) = w_d(i) + \frac{1}{\sqrt{PN}} \sum_n b_n \sum_{l=0}^{N_h-1} h_{iN+n,l} \times \sum_{\ell=-\infty}^{\infty} s_{\langle n-l \rangle_{PN}}(i-P\ell)\, a_{\ell PN+n-l} e^{-j\frac{2\pi}{PN}nd} \tag{5}$$

$$w_d(i) := \frac{1}{\sqrt{PN}} \sum_n b_n \nu_{iN+n} e^{-j\frac{2\pi}{PN}nd} \tag{6}$$

Frequency-domain equalization involves the i^{th}-frame *virtual subcarriers* $\{t_k(i)\}_{k=0}^{PN-1}$, where

$$t_k(i) := \frac{1}{\sqrt{PN}} \sum_{n=0}^{PN-1} s_n(i) e^{-j\frac{2\pi}{PN}nk}. \tag{7}$$

Equation (7) implies that $s_n(i) = \frac{1}{\sqrt{PN}} \sum_{k=0}^{PN-1} t_k(i) e^{j\frac{2\pi}{PN}nk}$ for $n \in \{0,\dots,PN-1\}$. Using this in (5) gives

$$x_d(i) = w_d(i) + \sum_{\ell=-\infty}^{\infty} \sum_{k=0}^{PN-1} t_k(i-P\ell) H_{d-k,k}(i,\ell) \tag{8}$$

$$H_{d,k}(i,\ell) := \frac{1}{PN} \sum_n \sum_{l=0}^{N_h-1} h_{iN+n,l} b_n a_{\ell PN+n-l}\, e^{-j\frac{2\pi}{PN}(kl+nd)} \tag{9}$$

Equation (8) indicates that $H_{d,k}(i,\ell)$ can be interpreted as the response, at DFT output $k+d$ in frame i, to a frequency-domain impulse applied at virtual subcarrier k in frame $i-\ell$.

In practice we implement a causal length-N_b window $\{b_n\}$ implying that, for any i, only a finite number of terms in the set $\{H_{d,k}(i,\ell), \ell \in \mathbb{Z}\}$ will be non-zero. Specifically, (9) implies that non-zero terms result from indices ℓ which satisfy $0 \le \ell NP + n - l \le PN-1$ for some $n \in \{0,\dots,N_b-1\}$ and some $l \in \{0,\dots,N_h-1\}$. It is straightforward to show that $H_{d,k}(i,\ell)$ is non-zero for $\ell \in \{-L_{\mathsf{pre}},\dots,L_{\mathsf{pst}}\}$ where $L_{\mathsf{pre}} = -\lfloor \frac{N_b-1}{PN} \rfloor$ and $L_{\mathsf{pst}} = \lfloor \frac{PN+N_h-2}{PN} \rfloor$.

Defining $[\boldsymbol{\mathcal{H}}(i,\ell)]_{d,k} := H_{d-k,k}(i,\ell)$ and $\boldsymbol{x}(i) := [x_0(i),\dots,x_{PN-1}(i)]^t$ and then defining $\boldsymbol{w}(i)$, $\boldsymbol{t}(i)$, $\boldsymbol{s}(i)$, and $\boldsymbol{\nu}(i)$ similarly, (8) implies the LTV vector model

$$\boldsymbol{x}(i) = \boldsymbol{w}(i) + \sum_{\ell=-L_{\mathsf{pre}}}^{L_{\mathsf{pst}}} \boldsymbol{\mathcal{H}}(i,\ell) \boldsymbol{t}(i-\ell P). \tag{10}$$

For any i, nonzero $\{\boldsymbol{\mathcal{H}}(i,\ell)\}_{\ell \neq 0}$ cause inter-frame interference (IFI) and nonzero off-diagonal elements of $\{\boldsymbol{\mathcal{H}}(i,0)\}$ cause inter-carrier interference (ICI) among the virtual subcarriers. In the sequel, we refer to $\{\boldsymbol{\mathcal{H}}(i,\ell)\}_{\ell<0}$ as pre-cursor IFI and $\{\boldsymbol{\mathcal{H}}(i,\ell)\}_{\ell>0}$ as post-cursor IFI.

The windowed frequency-domain noise vector can be written $\boldsymbol{w}(i) = \boldsymbol{C}\boldsymbol{\nu}(i)$ for $\boldsymbol{C} := \boldsymbol{F}\boldsymbol{J}\,\mathcal{D}(\boldsymbol{b})$, where $\boldsymbol{F}$ denotes the PN-point unitary DFT matrix and $\boldsymbol{J}$ a matrix whose j^{th} column equals $\boldsymbol{i}_{\langle j \rangle_N}$. We use this formulation in the sequel.

III. Max-SINR Window Design

The choice of window $\{b_n\}$ affects the IFI/ICI patterns of the system (10). Motivated by the low-pass nature of typical Doppler spectra, we aim to find $\{b_n\}$ such that the "cursor" coefficient $\boldsymbol{\mathcal{H}}(i,0)$ has the banded structure illustrated in Fig. 1 and the IFI coefficients $\{\boldsymbol{\mathcal{H}}(i,\ell)\}_{\ell \neq 0}$ vanish. This approach can be viewed as the frequency-domain dual of inter-symbol interference (ISI) response shortening used to reduce the complexity of maximum likelihood sequence detection (MLSD) [11]. For our purposes, the goal of time-domain windowing is to give the channel a sparse structure that leads to low-complexity estimation of $\boldsymbol{t}(i)$, and hence, low-complexity detection of $\boldsymbol{s}(i)$. We choose time-domain windowing, rather than a general matrix operation on the received signal, due to its low complexity. Since complete cancellation of out-of-target ICI/IFI is, in general, not possible with time-domain windowing, we choose to maximize signal to interference-plus-noise ratio (SINR) as a means of suppressing residual IFI/ICI.

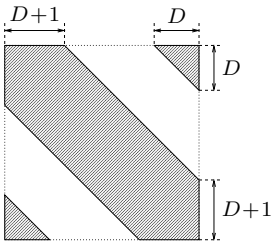

Fig. 1. Desired "banded" structure of matrix $\boldsymbol{\mathcal{H}}(i,0)$.

We define SINR by $\mathcal{E}_{\mathsf{s}}/\mathcal{E}_{\mathsf{ni}}$, where $\mathcal{E}_{\mathsf{s}} := \sum_d \mathcal{E}_{\mathsf{s},d}$ and $\mathcal{E}_{\mathsf{ni}} := \sum_d \mathcal{E}_{\mathsf{ni},d}$. For each $x_d(i)$, $\mathcal{E}_{\mathsf{s},d}$ is defined as the signal energy contributed by neighboring carriers $\{t_k(i)\}_{k=d-D}^{d+D}$, and $\mathcal{E}_{\mathsf{ni},d}$ is defined as the interference-plus-noise energy contributed by non-neighboring carriers $\{t_k(i)\}_{k=0}^{d-D-1} \cup \{t_k(i)\}_{k=d+D+1}^{PN-1}$, non-cursor carriers $\{t_k(j)\}_{j\neq i}$, and additive noise $\boldsymbol{w}(i)$. Note that indices here are taken modulo-PN. D is typically chosen as $D = \lceil f_{\mathsf{d}} T_{\mathsf{s}} PN \rceil$, where $f_{\mathsf{d}} T_{\mathsf{s}}$ is the maximum Doppler frequency normalized to the symbol rate. Using the approach outlined in [12], we find that the SINR-maximizing window $\boldsymbol{b}_\star$ is given by

$$\begin{aligned}\boldsymbol{b}_\star &= \arg \max_{\boldsymbol{b}:\|\boldsymbol{b}\|^2=1} \frac{\boldsymbol{b}^H(\boldsymbol{R}_b \odot \boldsymbol{D}_b \odot \boldsymbol{A}_{\mathsf{s}})\boldsymbol{b}}{\boldsymbol{b}^H(\sigma^2\boldsymbol{I} + \boldsymbol{R}_b \odot \boldsymbol{C}_b \odot \boldsymbol{A}_{\mathsf{t}} - \boldsymbol{R}_b \odot \boldsymbol{D}_b \odot \boldsymbol{A}_{\mathsf{s}})\boldsymbol{b}} \\ &= \boldsymbol{v}_\star\big(\boldsymbol{R}_b \odot \boldsymbol{D}_b \odot \boldsymbol{A}_{\mathsf{s}},\ \sigma^2\boldsymbol{I} + \boldsymbol{R}_b \odot \boldsymbol{C}_b \odot \boldsymbol{A}_{\mathsf{t}} - \boldsymbol{R}_b \odot \boldsymbol{D}_b \odot \boldsymbol{A}_{\mathsf{s}}\big)\end{aligned} \tag{11}$$

where $\boldsymbol{R}_b$, $\boldsymbol{A}_{\mathsf{s}}$, $\boldsymbol{C}_b$, $\boldsymbol{D}_b$ and $\boldsymbol{A}_{\mathsf{t}}$ are $N_b \times N_b$ matrices defined element-wise as $[\boldsymbol{R}_b]_{m,n} := \gamma_{n-m}$, $[\boldsymbol{A}_{\mathsf{s}}]_{m,n} := \sum_{l=0}^{N_h-1} \sigma_l^2 a_{n-l} a_{m-l}^*$, $[\boldsymbol{C}_b]_{m,n} := \delta_{\langle n-m\rangle_{PN}}$, $[\boldsymbol{D}_b]_{m,n} := \frac{1}{PN}\sin(\frac{\pi}{PN}(2D+1)(n-m))/\sin(\frac{\pi}{PN}(n-m))$ and $[\boldsymbol{A}_{\mathsf{t}}]_{m,n} := \sum_{\ell=-L_{\mathsf{pre}}}^{L_{\mathsf{pst}}} \sum_{l=0}^{N_h-1} \sigma_l^2 a_{\ell PN+n-l} a_{\ell PN+m-l}^*$. In (11), $\boldsymbol{v}_\star(\boldsymbol{B},\boldsymbol{C})$ denotes the principle generalized eigenvector [13] of the matrix pair $(\boldsymbol{B},\boldsymbol{C})$. With window (11) and proper selection of design parameters, the IFI and non-neighboring ICI can be made small enough to base the symbol detection procedure on the following approximate system model.

$$\begin{aligned}\boldsymbol{x}(i) &= \boldsymbol{\mathcal{H}}(i,0)\boldsymbol{t}(i) + \boldsymbol{C}\boldsymbol{\nu}(i), \\ \boldsymbol{t}(i) &= \boldsymbol{F}\boldsymbol{s}(i).\end{aligned} \tag{12}$$

As an alternative, the design parameters (e.g., frame length PN) could be chosen in such a way that post-cursor IFI is non-negligible. In this case, block decision-feedback equalization (BDFE) would be employed to cancel the effect of post-cursor IFI using the hard decisions $\{\hat{\boldsymbol{s}}(i-\ell P)\}_{\ell=1}^{L_{\mathsf{pst}}}$. With BDFE, the system model changes to

$$\boldsymbol{x}(i) = \boldsymbol{\mathcal{H}}(i,0)\boldsymbol{t}(i) + \sum_{\ell=1}^{L_{\mathsf{pst}}} \boldsymbol{\mathcal{H}}(i,\ell)\Big(\boldsymbol{t}(i-\ell P) - \boldsymbol{F}\hat{\boldsymbol{s}}(i-\ell P)\Big) + \boldsymbol{C}\boldsymbol{\nu}(i), \tag{13}$$

$$\boldsymbol{t}(i) = \boldsymbol{F}\boldsymbol{s}(i). \tag{14}$$

When we rely on BDFE to cancel the effect of post-cursor IFI, the window should be designed to suppress *only* ICI and pre-cursor IFI. In this case, post-cursor IFI would not be included in the definition of $\mathcal{E}_{\mathsf{ni}}$, implying $[\boldsymbol{A}_{\mathsf{t}}]_{m,n} := \sum_{\ell=-L_{\mathsf{pre}}}^{0} \sum_{l=0}^{N_h-1} \sigma_l^2 a_{\ell PN+n-l} a_{\ell PN+m-l}^*$. Figure 2 shows windows for the BDFE and non-BDFE cases at $f_{\mathsf{d}} T_{\mathsf{s}} \in \{0.001, 0.03\}$, Figure 2 assumed $N_h = 64$, $PN = 256$, $N_b = PN + N_h - 1$, SNR= 10dB, and $\sigma_l^2 = N_h^{-1}$, which are typical values for the numerical results in Sec. V.

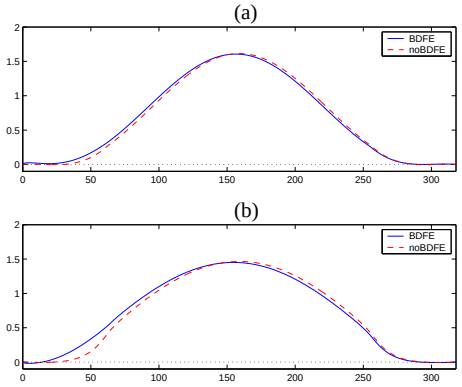

Fig. 2. Example window shapes for $PN = 256$, $N_h = 64$, SNR=10dB and (a) $f_{\mathsf{d}} T_{\mathsf{s}} = 0.001$, (b) $f_{\mathsf{d}} T_{\mathsf{s}} = 0.03$.

While windowing gives a sparse channel response that enables a reduced complexity symbol detection procedure, it can lead to a non-uniform collection of symbol energy across the observed frame. Specifically, it can be shown [14] that the energy in $\boldsymbol{x}(i)$ contributed by $s_n(i)$ is

$$\mathcal{E}_{\mathsf{ss},n} = \sum_{l=0}^{N_h-1} \sigma_l^2 |b_{l+n}|^2 \tag{15}$$

which is clearly dependent on n, the symbol position within the frame. This implies that, for typical max-SINR window shapes, symbols near the frame edges will contribute less energy than those in the center. This phenomenon motivates the symbol detection procedure proposed in Sec. IV.

IV. Symbol Detection

In Sec. IV-A we suggest an iterative method for the detection of the finite-alphabet symbol vector $\boldsymbol{s}(i)$ from observation $\boldsymbol{x}(i)$ specified by (12) or (13), in the non-BDFE and BDFE cases, respectively. Essentially, we borrow the detection algorithm from [8], which was developed for single-carrier systems *with* cyclic prefix (CP). With non-CP systems, however, the uneven collection of symbol energy is much more severe than with CP systems. Hence, Sec. IV-B proposes a scheme whereby frame overlap (i.e., $P > 1$) is exploited, in conjunction with the algorithm of Sec. IV-A, to circumvent these problems.

A. Intraframe Processing

We now give a brief summary of the intraframe detection algorithm that was developed in [8]. (Symbol and lag indices will be omitted since we focus exclusively on the i^{th} symbol and the cursor IFI coefficient.) Given current guesses of the log-likelihood ratios (LLRs) of the symbols $\{s_k\}$ (which, on the first iteration, are set to zero), the means and variances of the elements in $\boldsymbol{s}$ are calculated as $\bar{\boldsymbol{s}}$ and $\boldsymbol{v}$, respectively. These are then transformed into the mean and covariance of $\boldsymbol{t}$. Using linear MMSE estimation and incorporating these mean/variance priors, the elements $\{t_k\}$ are estimated one-at-a-time, leveraging the banded structure of $\boldsymbol{\mathcal{H}}$ for complexity reduction. The resulting estimates $\hat{\boldsymbol{t}}$ are then transformed back into the $\boldsymbol{s}$-domain, from which the LLRs are updated. To

$L_l^{(0)} = 0 \; \forall l$

for $n = 0, 1, 2, \ldots$

  for $l = 0 \ldots PN-1$,

    $\bar{s}_l^{(n)} = \tanh(L_l^{(n)}/2)$

    $v_l^{(n)} = 1 - (\bar{s}_l^{(n)})^2$

  end

  $\bar{\boldsymbol{t}}^{(n)} = \boldsymbol{F}\bar{\boldsymbol{s}}^{(n)}$

  for $k = 0 \ldots PN-1$,

    $\boldsymbol{g}_k^{(n)} = (\boldsymbol{\mathcal{H}}_k \boldsymbol{F} \mathcal{D}(\boldsymbol{v}^{(n)}) \boldsymbol{F}^H \boldsymbol{\mathcal{H}}_k^H + \sigma^2 \boldsymbol{C}_k \boldsymbol{C}_k^H)^{-1} \boldsymbol{\mathcal{H}}_k \boldsymbol{F} \mathcal{D}(\boldsymbol{v}^{(n)}) \boldsymbol{F}^H \boldsymbol{i}_k$

    $\hat{t}_k^{(n)} = \bar{t}_k^{(n)} + \boldsymbol{g}_k^{(n)H}(\boldsymbol{x}_k - \boldsymbol{\mathcal{H}}_k \bar{\boldsymbol{t}}^{(n)})$

  end

  $\hat{\boldsymbol{s}}^{(n)} = \boldsymbol{F}^H \hat{\boldsymbol{t}}^{(n)}$

  $\boldsymbol{Q}^{(n)} = \boldsymbol{F}^H \Big(\sum_{k=0}^{PN-1} \boldsymbol{\mathcal{H}}_k^H \boldsymbol{g}_k^{(n)} \boldsymbol{i}_k^H \Big) \boldsymbol{F}$

  $\boldsymbol{P}^{(n)} = \Big(\sum_{k=0}^{PN-1} \boldsymbol{C}_k^H \boldsymbol{g}_k^{(n)} \boldsymbol{i}_k^H \Big) \boldsymbol{F}$

  for $l = 0 \ldots PN-1$,

$$L_l^{(n+1)} = L_l^{(n)} + \frac{4 \left(\mathrm{Re}\{ Q_{l,l}^{(n)} (\hat{s}_l^{(n)} - \bar{s}_l^{(n)}) \} + |Q_{l,l}^{(n)}|^2 \bar{s}_l^{(n)} \right)}{\boldsymbol{q}_l^{(n)H} \mathcal{D}(\boldsymbol{v}^{(n)}) \boldsymbol{q}_l^{(n)} - |Q_{l,l}^{(n)}|^2 v_l^{(n)} + \sigma^2 \|\boldsymbol{p}_l\|^2}$$

  end

end

TABLE I

SUMMARY OF ITERATIVE SYMBOL ESTIMATION ALGORITHM.

accomplish this last step we assume a conditionally-Gaussian model for the estimates $\{\hat{s}_k\}$. The procedure then repeats, starting with the most recent LLRs.

Table I summarizes the algorithm detailed in [8], [14] for the BPSK case. In the table, n is used as the iteration index and l as the symbol index. Also, $L_l^{(n)}$ denotes the LLR, $\bar{\boldsymbol{t}}^{(n)}$ the mean of $\boldsymbol{t}^{(n)}$, $\boldsymbol{x}_k := [\boldsymbol{x}]_{k-D:k+D}$, $\boldsymbol{\mathcal{H}}_k := [\boldsymbol{\mathcal{H}}]_{k-D:k+D,k-2D:k+2D}$, $\boldsymbol{C}_k := [\boldsymbol{C}]_{k-D:k+D,:}$, $Q_{l,l}^{(n)} := [\boldsymbol{Q}^{(n)}]_{l,l}$, $\boldsymbol{q}_l^{(n)} := [\boldsymbol{Q}^{(n)}]_{:,l}$, and $\boldsymbol{p}_l^{(n)} := [\boldsymbol{P}^{(n)}]_{:,l}$, with indices taken modulo-PN. See [8], [14] for fast implementations of the algorithm (that avoid explicit computation of $\boldsymbol{Q}^{(n)}$, $\boldsymbol{P}^{(n)}$).

B. Interframe Processing

As seen in (15), the symbols in the center of $\boldsymbol{s}(i)$ contribute more energy to the observation $\boldsymbol{x}(i)$ than those near the edges. As a result, the iterative detection algorithm described in Sec. IV-A may generate *relatively* high error rates for the edge symbols in $\boldsymbol{s}(i)$. However, when overlapping frames are used (i.e., $P > 1$), this problem can be circumvented by exploiting the fact that every symbol will be near the center of some frame. Specifically, (3) implies that s_m appears in P distinct frames. The frame index i_m for which s_m appears closest to frame center is readily found to be $i_m = \left\lfloor \frac{m}{N} \right\rfloor - j_m$ for $j_m := \arg\min_{j=0,\ldots,P-1} \left| \langle m \rangle_{N} + jN - \frac{PN}{2} \right|$. Thus, to exploit frame overlap, we stipulate that

1) the hard estimate of s_m is generated at frame index i_m,
2) the final LLR calculated for symbol s_m during frame i_m is used to initialize the LLR of that symbol in subsequent frames within which it appears.

In the case that BDFE is employed, these hard estimates are then also used for post-cursor IFI cancellation. Figure 3 illustrates this process for $P = 2$.

Since every symbol s_m is estimated P times, the overall equalizer complexity increases linearly with P. Numerical simulations suggest that the performance with $P > 2$ is not significantly better than $P = 2$, while the performance with $P = 1$ is relatively poor. Hence, we focus on $P = 2$.

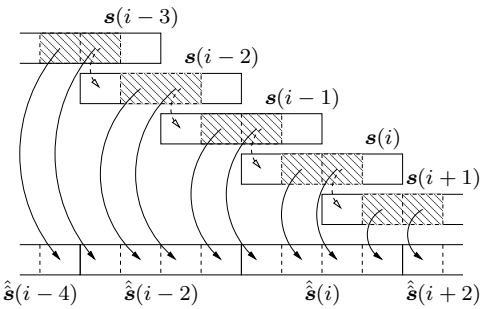

Fig. 3. Interframe detection process for $P = 2$. Solid arrows pass final hard estimates; dashed arrows pass soft initializations.

V. NUMERICAL RESULTS

In this section we compare the performance and complexity of the fast iterative frequency domain equalization (IFDE) algorithm summarized in Table I with the well known FIR-MMSE-DFE. While the FIR-MMSE-DFE was originally derived for LTI channels [15], it is straightforward to generalize the algorithm to LTV channels, and possible to design a recursive algorithm to update the filter coefficients at the symbol rate assuming a fixed delay Δ [14]. In all simulations, BPSK symbols are transmitted over a noisy WSSUS Rayleigh fading channel with uniform power profile (i.e., $\sigma_l^2 = N_h^{-1}$) that is generated using Jakes method [16]. Throughout, we assume IFDE uses an ICI radius of $D = \lceil f_{\mathsf{d}} T_{\mathsf{s}} PN \rceil$ and frame overlap factor of $P = 2$. Both IFDE and FIR-MMSE-DFE designs are based on perfectly known time-domain channel.

First, we establish IFDE-BDFE design rules for frame length PN and number of iterations M. While we will see that smaller values of PN (for fixed N_h) are advantageous from a complexity standpoint, experiments suggest setting $PN \geq 4N_h$ to avoid performance degradation. With radix-2 FFTs in mind, we choose $PN = 2^{\lceil \log_2 4N_h \rceil}$ in the sequel. We found that performance increases with the number of iterations M (as would be expected) up to about $M = 10$, after which there is little improvement. Interestingly, we find that, after 2 iterations, IFDE-BDFE gives approximately the same performance as FIR-MMSE-DFE (see Fig. 4). Hence, we focus on IFDE-BDFE-2 and IFDE-BDFE-10 in the sequel.

For the FIR-MMSE-DFE, we use a feedback filter just long enough to cancel all post-cursor ISI, a forward filter length equal to the channel delay spread, and a delay equal to the forward filter length minus one. These design rules were the result of a detailed study in [14].

Having established IFDE-BDFE and FIR-MMSE-DFE design rules, we are ready to compare the two approaches in performance and complexity. In Fig. 4, we compare SER performances when $N_h = 64$ and $f_{\mathsf{d}} T_{\mathsf{s}} \in \{0.001, 0.01, 0.03\}$ over a wide range of SNR. Note that, at all $f_{\mathsf{d}} T_{\mathsf{s}}$, IFDE-BDFE-2 performs equivalently to FIR-MMSE-DFE whereas IFDE-BDFE-10 outperforms FIR-MMSE-DFE, significantly so when SNR> 5. We also plot the matched-filter bound

(MFB) [10]—the ultimate receiver performance—which is not far from IFDE-BDFE-10.

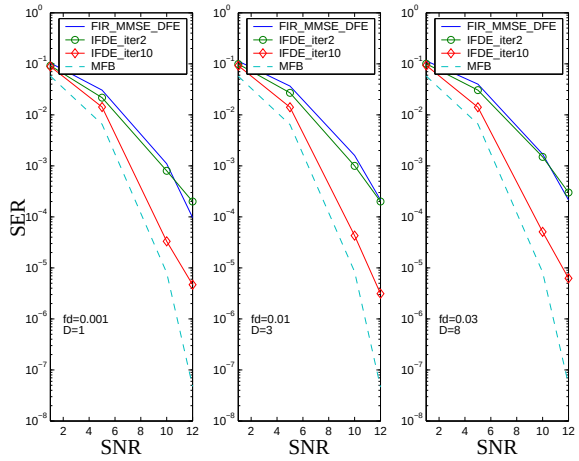

Fig. 4. Symbol error rate versus SNR for $N_h = 64$ and various $f_\mathsf{d}T_\mathsf{s}$.

Figure 5 examines the multiplies-per-symbol ratio of FIR-MMSE-DFE to IFDE-BDFE-2 using the results of a complexity analysis in [14]. Note that values > 1 in Fig. 5 imply a complexity *advantage* for IFDE-BDFE, and that this complexity advantage increases with N_h and decreases with $f_\mathsf{d}T_\mathsf{s}$. Since FIR-MMSE-DFE and IFDE-BDFE-2 have similar performance, Fig. 5 constitutes a direct *complexity* comparison. We show in [14] that IFDE-BDFE-10 requires roughly three times the computation of IFDE-BDFE-2, and thus (recalling Fig. 4) beats FIR-MMSE-DFE in performance *and* computation over a wide range of $(N_h, f_\mathsf{d}T_\mathsf{s})$.

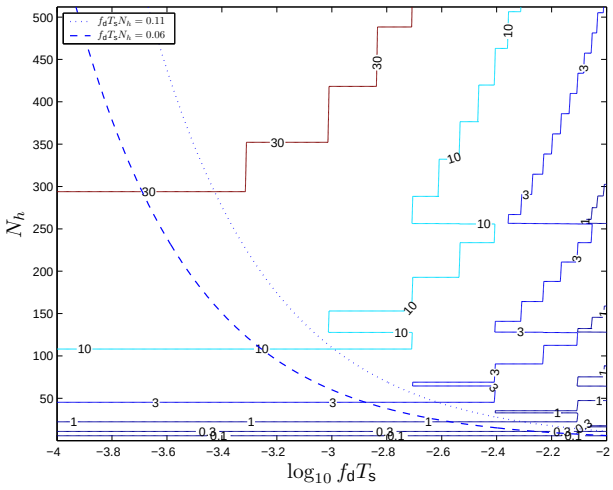

Fig. 5. Complexity of FIR-MMSE-DFE relative to IFDE-BDFE-2.

A final comment regarding the complexity comparison Fig. 5 is in order. One could argue that the FIR-MMSE-DFE, which—for our LTV channels—calculates a filter update *every* symbol period, is "overkill" for slowly varying channels. For these channels, decent performance should result from approximating the LTV channel response as *fixed* over, say, N_f symbol intervals and designing a single fixed MMSE-DFE to operate over this N_f-symbol interval based on Toeplitz channel matrices. The question is, then, for what range of $(f_\mathsf{d}T_\mathsf{s}, N_h)$ will the channel be "slow enough" for this block-LTI approximation to hold? Numerical experiments at SNR= 10dB have shown that this block-LTI approximation results in an equivalent SNR *loss* of at least 3dB when $f_\mathsf{d}T_\mathsf{s}N_h > 0.11$ and a loss of at least 1dB when $f_\mathsf{d}T_\mathsf{s}N_h > 0.06$ [14]. Note the curves $f_\mathsf{d}T_\mathsf{s}N_h = 0.11$ and $f_\mathsf{d}T_\mathsf{s}N_h = 0.06$ on Fig. 5.

VI. Conclusion

In this paper, we presented an iterative frequency domain equalization (IFDE) scheme for single-carrier transmissions over noisy doubly-dispersive channels. Time-domain windowing is used make the effective ICI/IFI response sparse, after which iterative symbol estimation is performed in the frequency domain. The estimation algorithm leverages the finite-alphabet property of symbols, the sparse ICI/IFI structure, and the low computational cost of the FFT. Simulations demonstrated that IFDE performs significantly better than the FIR-MMSE-DFE, while simultaneously offering significant complexity savings, for long delay-spread channels.

References

[1] S. B. Weinstein and P. M. Ebert, "Data transmission by frequency division multiplexing using the discrete Fourier transform," *IEEE Trans. Commun.*, vol. 19, pp. 628–634, Oct. 1971.

[2] D. Falconer, S. L. Ariyavisitakul, A. Benyamin-Seeyar, and B. Eidson, "Frequency domain equalization for single-carrier broadband wireless systems," *IEEE Commun. Mag.*, vol. 40, pp. 58–66, Apr. 2002.

[3] T. Walzman and M. Schwartz, "Automatic equalization using the discrete frequency domain," *IEEE Trans. Inform. Theory*, vol. 19, pp. 59–68, Jan. 1973.

[4] A. Stamoulis, S. N. Diggavi, and N. Al-Dhahir, "Intercarrier interference in MIMO OFDM," *IEEE Trans. Signal Processing*, vol. 50, pp. 2451–2464, Oct. 2002.

[5] X. Cai and G. B. Giannakis, "Bounding performance and suppressing inter-carrier interference in wireless mobile OFDM," *IEEE Trans. Commun.*, vol. 51, pp. 2047–2056, Dec. 2003.

[6] A. Gorokhov and J.-P. Linnartz, "Robust OFDM receivers for dispersive time-varying channels: Equalization and channel acquisition," *IEEE Trans. Commun.*, vol. 52, pp. 572–583, Apr. 2004.

[7] P. Schniter, "Low-complexity equalization of OFDM in doubly-selective channels," *IEEE Trans. Signal Processing*, vol. 52, pp. 1002–1011, Apr. 2004.

[8] P. Schniter and H. Liu, "Iterative equalization for single carrier cyclic-prefix in doubly-dispersive channels," in *Proc. Asilomar Conf. Signals, Systems and Computers*, Oct. 2003.

[9] I. Barhumi, G. Leus, and M. Moonen, "Frequency-domain equalization for OFDM over doubly-selective channels," in *Proc. Baiona Workshop on Signal Processing in Commun.*, Sept. 2003.

[10] J. G. Proakis, *Digital Communications*. New York: McGraw-Hill, 4th ed., 2001.

[11] D. D. Falconer and F. R. Magee, "Adaptive channel memory truncation for maximum likelihood sequence estimation," *Bell System Tech. J.*, vol. 52, pp. 1541–1562, Nov. 1973.

[12] P. Schniter, "A new approach to multicarrier pulse design for doubly-dispersive channels," in *Proc. Allerton Conf. Commun., Control, and Computing*, Oct. 2003.

[13] G. H. Golub and C. F. Van Loan, *Matrix Computations*. Baltimore, MD: John Hopkins University Press, 3rd ed., 1996.

[14] P. Schniter and H. Liu, "Iterative frequency-domain equalization of single-carrier transmissions over doubly-dispersive channels," (Journal manuscript in preparation).

[15] N. Al-Dhahir and J. M. Cioffi, "MMSE decision feedback equalizers: Finite-length results," *IEEE Trans. Inform. Theory*, vol. 41, pp. 961–976, July 1995.

[16] W. C. Jakes, *Microwave Mobile Communications*. Wiley, 1974.